Fachtagung "Lasermethoden in der Strömungsmesstechnik"
8. – 10. September 2015, Dresden

On the Global Behavior of the Flow Field in a Transparent Experimental Model of a Hard Disk Drive

Shohei Ishimura, Katsuaki Shirai, Ryo Tada, Tsuyoshi Kawanami, Shigeki Hirasawa
Laboratory of Energy Conversion Engineering
Department of Mechanical Engineering
Kobe University
Rokkodai 1-1, Nada, Kobe, 657-8501, Japan
shirai@mech.kobe-u.ac.jp

Keywords: Hard Disk Drive, Rotating Flow, Refractive Index Matching, Particle Image Velocimetry

Abstract

Hard disk drives (HDDs) are widely used as a major device for data storage. Besides the higher areal density and lower power consumption demanded in the next-generation HDDs, their reliability still remains an important issue to secure the data. The reliability is hindered by the crash of the magnetic head against the disk surface. However, exact mechanism of the crash has not been understood and hence there is no versatile solution to prevent it. We investigate the complex flow behavior of the flow inside a HDD in order to clarify the mechanism responsible for inducing the crash. We created a simplified HDD model equipped with a read-and-write assembly (RWA) and a shroud opening. A scaled experimental model was built with all the parts made of a transparent material. A refractive index matching was applied to the working fluid so that the whole parts became optically transparent while they maintain their mechanical functions. A series of flow visualizations were carried out at different conditions of Reynolds number, the insertion angle of the RWA and the observation planes. We also performed a measurement of the planer velocity field using a particle image velocimetry (PIV). We report on the global behavior of the flow based on the flow visualization and the PIV measurement.

1. Introduction

Hard disk drives (HDDs) have been widely used as data storage device. A general HDD consists of a stack of rotating disks with a revolution ranging from 5400 rpm to 7200 rpm and a read-and-write assembly (RWA). A magnetic head equipped at the top of the RWA reads and writes data on the disk surface. The head fly over the disk surface due to the lift force induced by the disk revolution. The fly height is precisely controlled by servo mechanism for less than a few nanometers. The development of HDDs continues toward achieving higher areal density with lower energy consumption. Their reliability remains an important issue to secure the data stored in the HDDs. For the rare occasion, the magnetic head collides against the disk surface. The crash is a fatal problem that results in the loss of data. So far, there are two possible scenarios which are supposed to be responsible for the crash. One is the vibration induced by the complex air flow [1]. The vibration amplitude of the disks was reported to decrease when the tip clearance between the disk to the shroud wall became narrower [2]. Another is the collision of a particle against the magnetic head. A particle wandering in the drive may induce an impact when it collides against the head. However, the exact mechanism of the crash has not been understood. In any case, the internal flow must play a key role in the crash mechanism. Hence, investigation of the complex flow behavior is vital in order to clarify the crash mechanism and to prevent it.

On the flow inside HDDs, many investigations have been done both in experiments and numerical simulations. They provided several common findings on the flow between the disks. In a plane parallel to the disks, the inner region exhibits solid body rotation while large scale vortices are formed in the outer region [3]. The inner region forms polygonal shaped structure and the shape changes depending on the Reynolds number and the aspect ratio of the disk-to-disk spacing to the disk radius. On the other hand, secondary flow structure is observed in the cross-sectional plane (vertical to the disks). The complex flow was classified into three different regimes [5]. However, most of the works have been done using excessively simplified models, typically a stack of rotating disks mounted in an axisymmetric enclosure without an RWA. It is questionable to apply the findings from such a simple axisymmetric geometry to understand the flow behaviors in real HDDs with a non-axisymmetric geometry and an RWA inserted between the disks. More recently, velocity measurements in the narrow spaces were attempted using a model with a non-axisymmetric enclosure with an RWA [6], but the stagnation flow in the shroud opening was not properly reproduced. Numerical simulations of HDD flows have been performed using the design geometry of a specific HDD [7]. In spite of the spread of simulating tools, numerical simulation of the flow is still challenging because of the need to resolve a wide range of the scales existing in HDDs. Besides, it is also difficult to obtain sufficient amount of the statistics in numerical simulations.

We constructed a new HDD model in order to understand the common features of the flow. The model contains a pair of rotating disks with a simulated RWA placed in a non-axisymmetric enclosure. It has a still simplified geometry but was designed to represent common geometric features of a HDD. Our intension is not to stick on a specific geometry design of a particular product but to understand the flow physics common to HDDs in general. We performed a series of flow visualization experiments based on the proposed model. In the visualization, a refractive index matching (RIM) was applied to the scaled experimental model so that the whole area of the model became optically transparent with the functionality of the parts remained. Three-dimensional flow behavior has been observed and regions with strong shear were found in the visualization. However, the study was limited to qualitative examination and quantitative evaluation of the flow filed was expected.

In the present study, we extended the qualitative visualization into quantitative measurement. We used the scaled experimental model under a RIM condition. We built a measurement system of two-dimensional planar particle image velocimetry (PIV). Measurements were made on the velocity fields in the planes parallel to the disks. In the following, we report on the experiment and some early results obtained in the PIV measurement. We focus on the global behavior of the flow.

2. Flow Analogy and Scaling

We chose Reynolds number as the primary similarity parameter among others since we focus on the flow dynamics of a HDD. Besides, it is impossible to keep the similarities of flow and other phenomena. The disk Reynolds number is defined as

$$Re = \frac{\rho R_2 \Omega \left(R_2 - R_1\right)}{\mu}, \tag{1}$$

where ρ is the fluid density, R_1 the hub radius, R_2 the disk radius, Ω the disk angular velocity and μ the viscosity. In addition to the dimensions parallel to the disks, those perpendicular to

the disks also give influences the flow behavior. The parameters were non-dimensionalized with the tangential velocity at the outer edge of the disk and the inter-disk spacing

$$h = \frac{H}{R_2},\ z^* = \frac{z}{H},\ v^* = \frac{v}{r\,\Omega},\ r^* = \frac{r}{R_2}, \tag{2}$$

where *H* is the inter-disk spacing (i.e., the disk-to-disk distance), *z* the axial coordinate (the datum level on the middle plane between the disks), *r* radial direction and *v* the flow velocity.

3. HDD Model

The HDD model consisted of a pair of disks and a stack of simplified RWAs mounted in a non-axisymmetric enclosure as shown in Fig. 1 (a). A large shroud opening was equipped so that the flow stagnation got properly reproduced in the region (see the bottom right of Fig. 1 (a)). The experimental model was a 2:1 scale of a 3.5 inch HDD for desk top computers. This scale was determined in order to match the Reynolds number in Eq;(1) in the experiment. The RWA is alternately inserted into the spaces between the top-to-disk, disk-to-disk and disk-to-bottom of a non-axisymmetric enclosure as depicted in Fig. 2. The disks had a radius of 100 mm, a thickness of 3 mm and the inter-disk space is 6 mm. The RWA had a thickness of 3 mm with the disk being spaced 1.5 mm apart from the RWA. The thickness values of these components were intentionally made more than twice those of the scaled value by taking into account of their stiffness. Otherwise, the disks would bend inward by the low pressure conditions at fast rotations of the disks [6]. With the present thickness values, we have not observed any bend of the components in the present experiment. The RWA was placed in a way that the insertion angle was set at different angles as illustrated in Fig. 3. The insertion angles correspond to the head reading/writing data at the different radial tracks on the disks. The experimental model was made of a transparent material, i.e., poly-methyl methacrylate (PMMA). The parts were all made of a sane PMMA material including the enclosure, disks, hubs, RWAs and rotating shaft, except for the bearing and liquid seal.

In the present study, we aimed to have an unobstructed optical view in the whole area of the flow in the model. In order to realize such a view, a RIM technique is known [8]. A RIM technique minimizes shadows and glare points occurred at the boundaries of solid and fluid. The working fluid was carefully chosen for realizing a RIM in the experiment. The refractive index of the working fluid was adjusted to that of the solid parts made of PMMA (refractive index: 1.49). The ternary solution consists of ammonium thiocyanate, glycerin and water. As a result, all the parts including the fluid and solid inside whole the enclosure became optically transparent while their mechanical functions were maintained. The effect of the index matching was significant as shown in Fig. 1 (b, c). The solution was found to be stable for over weeks once it was created.

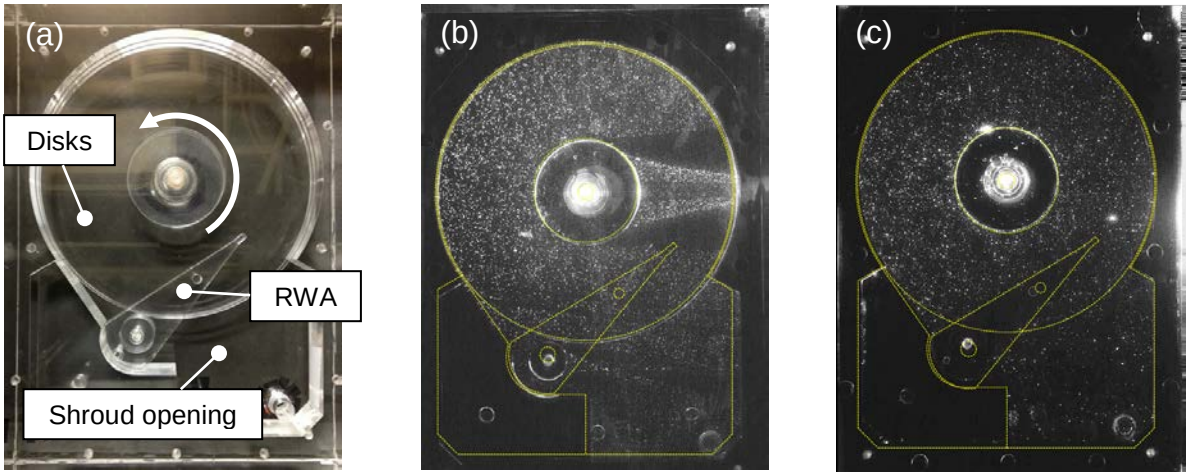

Fig. 1: The HDD model and typical images at the experiment with/without refractive index matching, (a) picture of the HDD model, (b) image with non- index matched fluid (water), (c) with the index matched fluid (aqueous solution of ammonium thiocyanate and glycerin).

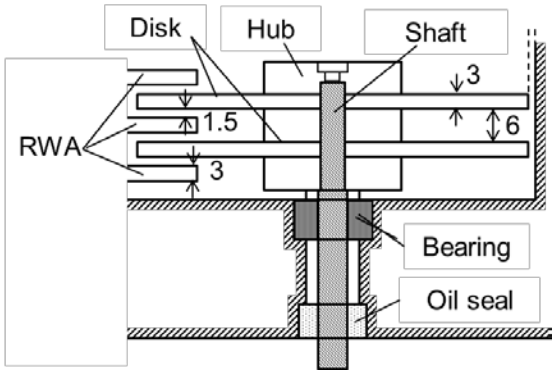

Fig. 2: Cross-sectional view of the design of the present HDD model.

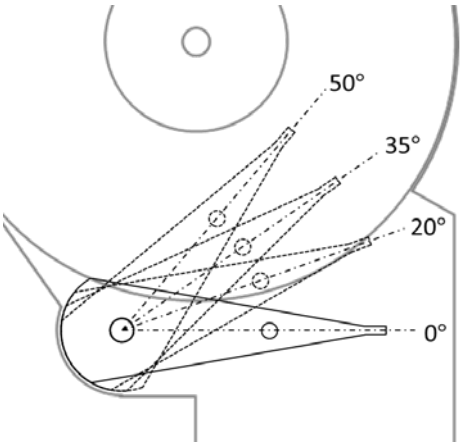

Fig. 3: The angle definition of the RWA insertion to the flow (0°, 20°, 35°, 50°).

4. Experimental Apparatus and Conditions

4.1 Apparatus

The PIV system consisted of a double-pulsed laser, optics forming the light sheet, a function generator, a pulse-delay generator, a CCD camera (1392×1040 pixels, 14 bit, mono-chrome, double shutter) and a computer as illustrated in Fig. 4. Ion exchange resin (mean diameter: 100 μm, density: 1.01 g/cm^3) was seeded as tracer particles in the flow. In a preliminary consideration, we confirmed the particle tractability to the flow in terms of buoyancy, centrifugal and lift forces. The laser (Nd:YAG, 532 nm, 20 mJ/pulse, pulse width: 5~9 ns) consisted of two independent heads. The timing control of the system was realized with a function generator and a pulse-delay generator connected to each of the laser drivers and the camera. The laser beams were guided through the optics and converted into light sheets. The HDD model was illuminated by the light sheet from the side. The light sheet was about 1.5 mm thick. For calculating the velocity vectors from the image pairs, cross-correlation algorithm was applied. An open-source software PIVlab was utilized for the analysis.

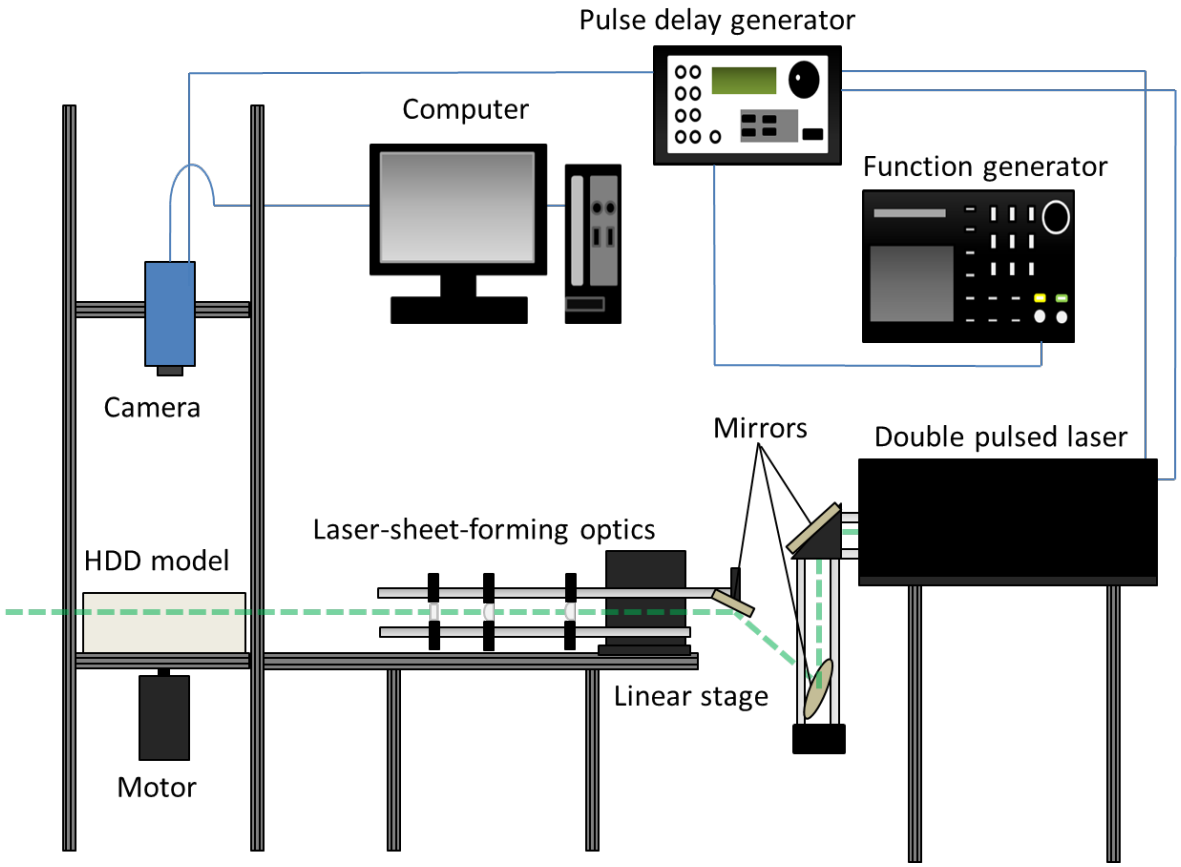

Fig. 4: Overview of the experimental setup at the PIV measurement, consisting of a double-pulsed laser, optics, a function generator, a pulse-delay generator, a CCD camera and a computer.

4.2 Measurement conditions

PIV measurements were performed at four insertion angles (0°, 20°, 35°, 50°) at two planes (z^*= 0 and 0.42) shown in Fig. 3 and Fig. 5. The angular velocity was set to 296 rpm (the disk Reynolds number: 4.8×10^4), which corresponded to 5400 rpm in a real 3.5 inch HDD. The size of the interrogation window was set to 64×64 pixels with 50% overlap. The resulting spatial resolution became about 200×200 μm^2. The interval between image pairs was set to 200 ms taking into account of the one-quarter rule of in-plane PIV analysis [4], which corresponded to approximately 1 image pair acquisition per revolution. This ensures the statistical independence of the image pairs.

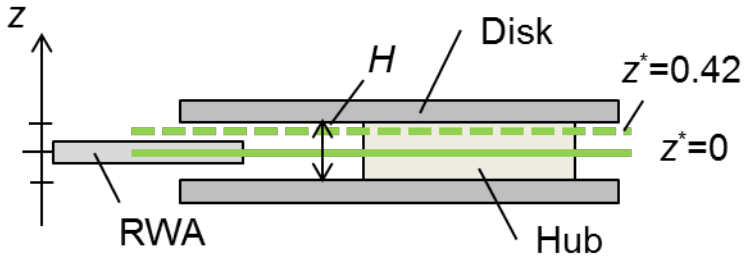

Fig. 5: Definition of the illumination planes of the laser sheet.

5. Results and Discussions

5.1 Rotating flow in the disk area

Velocity magnitude at the disk middle plane (z^*=0) are shown in Fig. 6. Each of these images is the average of 200 images, respectively. Laser sheet was irradiated from the left side in the images. In the disk area, flow velocity decreases as the RWA inserted deeply into the inner region. The maximum velocity decreased about 0.6 m/s at the insertion angles from 0° and 50°. At the angles of 0°and 20°, there are distinct annular region of high velocities seen between the hub and the shroud. Fig. 7 shows the velocity profiles normalized by Eq.(2) along the line OD located in the opposite of the shroud opening (see Fig. 7 (a) for the line). The normalized velocity profiles for the four angles exhibit similar trend as shown in Fig. 7 (b). In the inner region, the normalized velocities have constant values, indicating the solid-body rotation. The velocities become slightly larger than the local tangential velocities on the disk. Toward the outer region, the velocities decreases start to decrease and finally down to 40 to 65 percent of the local tangential velocities on the disk. The velocities have a very similar behavior for the cases of 0°and 20°. In the same figure, we show the result of Schuler et al. (1990), who measured the velocities using a laser Doppler anemometry (LDA) [5]. The normalized velocity profiles obtained in the present study are consistent to their result despite their results were obtained by using an axisymmetric enclosure without an RWA. This similarity is attributed to the fact that the blockages by the RWA in the cases of 0°and 20° were similar to the flow geometry in an axisymmetric enclosure without an RWA. Beyond at a certain angle, the obstruction of the flow became larger and the resulting flow structure starts to be influenced by the non-axisymmetric geometry. In the cases of 35°and 50°, the annular shaped high velocity regions seen in the 0°and 20° disappear. Instead, the high velocity regions exist locally near the RWA not extended to circulate. There are two regions of high velocities in the cases of 35°and 50°. The primary one is seen in the inner side of the RWA. It was created by the blocking and narrowing effects of the flow path by the RWA. The flow behaves locally like a jet from a nozzle in the region. The secondary regions observed behind the RWA are less discernible. The region seems to be caused by some part of the flow which circumvented the RWA. It merges with the primary region just in the downstream of the RWA. Some small eddies shed in the region were reported in the prior research with a flow visualization, but those eddies have not captured by the PIV measurement probably caused by the low resolution using the interrogation-window size of 64×64 pixels.

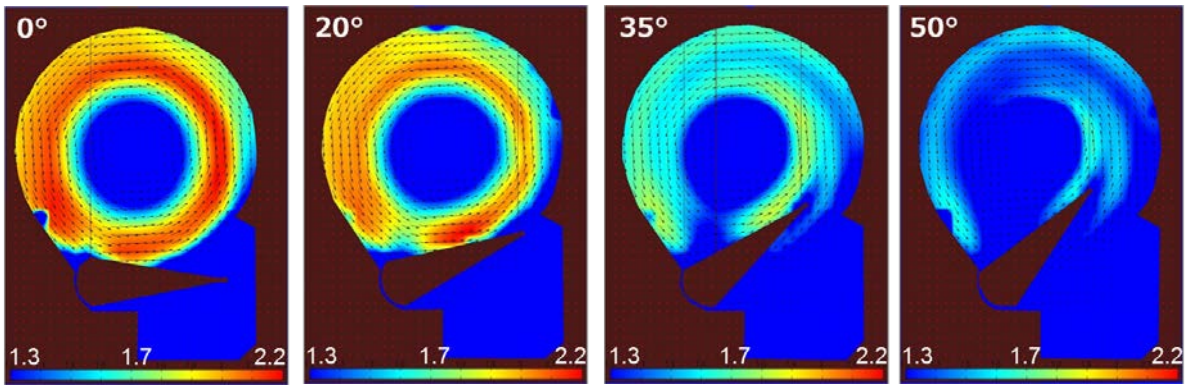

Fig. 6: Velocity magnitude at the middle plane including the arm (z^*=0).

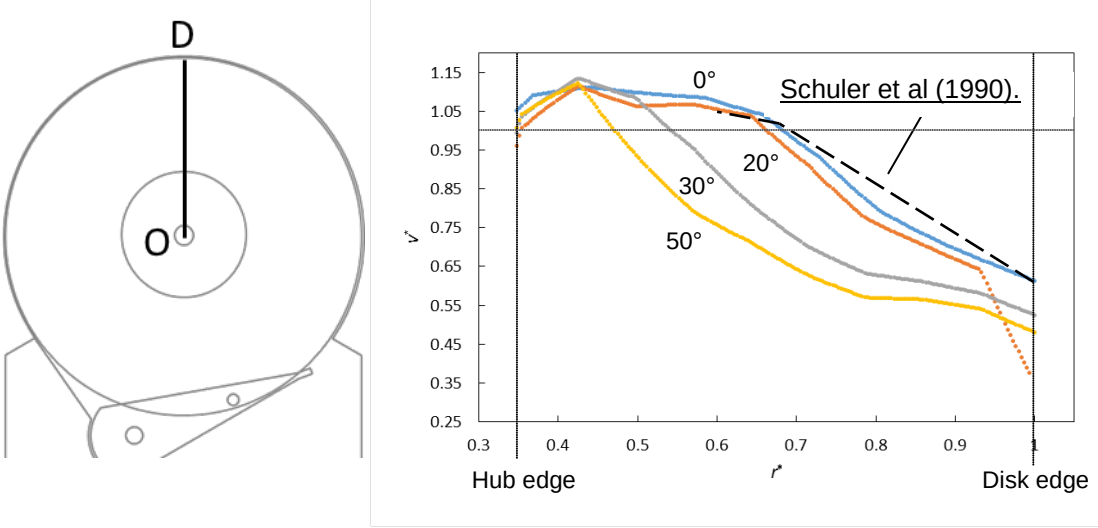

Fig. 7: The polyline along which velocity data was extracted (the left image). The graph showing relationship between non-dimensionalized velocity and radius (the right image). The line signifies 0°, 20°, 35° and 50° in order from the top.

Fig. 8 shows vorticity fields in z^*=0 plane. Vorticity means the degree of flow to rotate, described by

$$\omega_z = \frac{\partial v}{\partial x} - \frac{\partial u}{\partial y} \quad , \tag{3}$$

in a two-dimensional flow. In the color contour, the red (the positive) represents the clockwise curl and the blue (the negative) represents the counter-clockwise curl. The vorticity became positively large in the interface region between the disk and the shroud opening area regardless of the RWA angles. This positively large vorticity is caused by the high velocities in the disk area (see Fig. 6 and the above discussion) interfaces the small velocities in the shroud opening area. The substantial velocity difference between the two areas was expected from the prior flow visualization and the fluid with small velocities in the shroud opening region entrains into the disk area. Further investigation on the region is expected to examine the strong shear and its influences in the downstream. Fig. 9 shows vorticity fields at the plane between the disk and the RWA (z^*= 0.42). The vorticities in this plane exhibit similar tendency to the disk middle plane for all the four RWA angles. However, the vorticity was found to become negatively large at the trailing edge near the hole equipped with the RWA. On the other hand, vorticity was positively large at the leading edge where the flow hit against the RWA.

5.2 Stagnation flow in the shroud opening

We focus on the shroud opening area where the flow is expected to be almost stagnates. Fig. 10 shows the resulting velocity magnitudes in the upper row and vorticity fields in the lower row. In the area, the incoming flow enters into the large opening area similar to the flow with a backward facing step. The flow separates at the rear edge of the block and forms a large clockwise recirculation. The incoming fluid flowing against the wall bifurcates into upper and lower directions. The upper flow gradually flows back into the disk area while the lower flow flows along the wall to create the flow recirculation. The flow was almost stagnant at the case of 0°while it exhibit strong recirculation region at the case of 50°. As the RWA angle becomes deeper, the incoming flow enters from the pivotal region of the RWA with faster velocities and

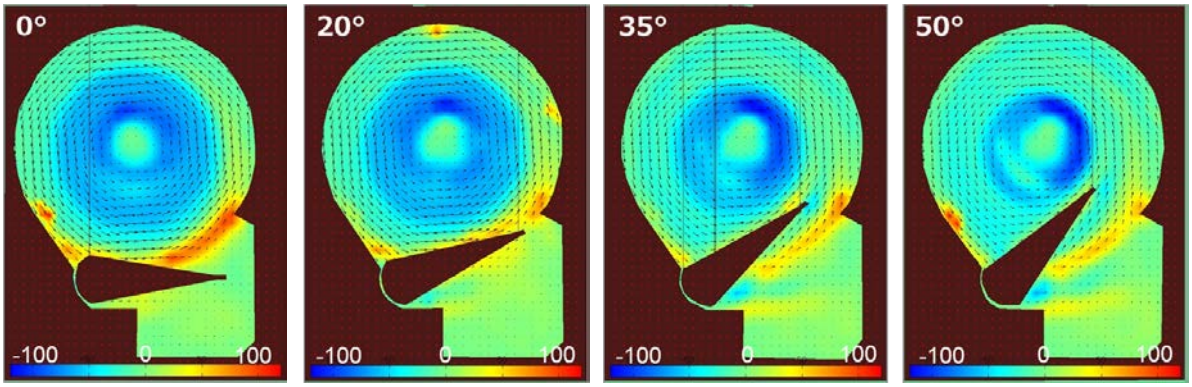

Fig. 8: Vorticity fields at the middle plane including the arm (z^*=0).

they become more diffusive. The flow rate of the incoming flow is increased by the amount of area blocked by the insertion of the RWA. Concerning the vorticities, their magnitude increases as the increase of the RWA insertion angle. Especially, they become prominent at the angles of 35 and 50°. The negative vorticity originates from the flow winds around the pivot after passing along the curved gap between the pivot and the shroud. Regions of positive vorticity are observed near the disk edge as discussed in the section 5.1. The positively large vorticity from the rear edge of the block corresponds to the recirculating flow in the bottom part of the shroud opening area as discussed above. Besides, pairs of positive and negative vorticity pairs are seen in the upper side of the shroud opening area. This vorticity behavior with the counter rotating vorticity pairs may have arisen from the Kármán vortex streets shed from the pivotal shaft for fixing the RWA in the upstream. Further investigation is required on this point.

6. Summary

The complex flow was investigated on the internal flow of the HDD model. The model was equipped with a RWA and a shroud opening to investigate the influence of the RWA insertion and the stagnating flow in the shroud opening. We focused on the global flow of the whole area inside the scaled HDD model by applying a RIM to the working fluid. Quantitative evaluation of the velocity field was performed based on the PIV analysis. The velocity magnitudes and the vorticity fields were examined at the two observation planes with four RWA angles. In the disk area. The rotating flow in the disk area was disturbed by the RWA. The blockage by the RWA induces high velocity regions and the influence of the RWA increases with the insertion angle. In the shroud opening area, the incoming flow becomes stagnant. A part of the flow recirculates in the bottom area and the other part gradually flows back and merges

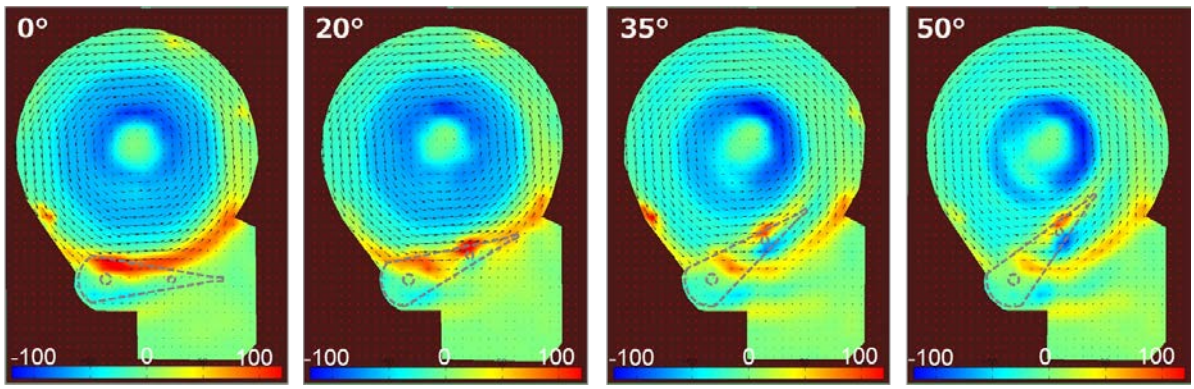

Fig. 9: Vorticity fields at the plane between the disk and the arm (z^*= 0.42)

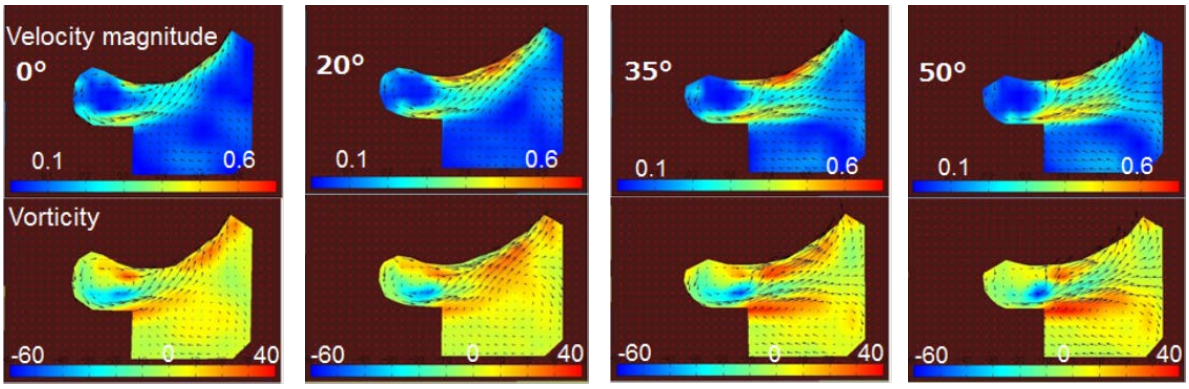

Fig. 10: Velocity magnitude (upper row) and vorticity fields (lower row) in the shroud opening area at the plane between the disk and the arm (z^*= 0.42).

into the fast flow in the disk region. The recirculating flow formed in the area becomes prominent as the arm insertion angle increase. Resolution, reproducibility and statistical reliability need to be investigated. Further measurement is conducted for the evaluation of turbulence statistics including Reynolds shear stress components and turbulent kinetic energy.

Acknowledgements

The present study has been partially supported by the Storage Research Consortium (SRC), the Strategic Basic Research Programs (the Advanced Low Carbon Technology Research Development Program) of the Japan Science and Technology Agency, and the Kakenhi Grants (24860041, 26820048) of the Japan Society for the Promotion of Science. The authors greatly acknowledge these supports.

References

[1] Takada, S., Kusukawa, T., Tagawa, N., Mori, A., Mizoh, Y., Nakakita, M., 2007: “Study on flow-induced vibration of head-disk assembly mechanisms in actual hard disk drive”, Microsyst Technol, Vol. 13, pp.767-775.
[2] Imai, S., Tokuyama, M., Yamaguchi, Y., 1999: “Reduction of Disk Flutter by decreasing disk-to-shroud spacing”, IEEE Trans. Magnet., Vol. 35, pp.2301-2303.
[3] Abrahamson, S. Eaton, J.K., Koga, D.J., 1989: “The flow between shrouded corotating disks”, Phys. Fluids A, Vol. 1, pp. 241-251.
[4] Schuler, C.A., Usry, W., Weber, B., Humphrey, J.A.C., Greif, R., 1990: “On the flow in the unobstructed space between shrouded co-rotating disks”, Phys. Fluids, Vol. 2, No. 10, pp. 1760-1770.
[5] Herrero, J., Giralt, F., Humphrey, J.A.C., 1999, “Influence of the geometry on the structure of the flow between a pair of corotating disks”, Phys. Fluids, Vol. 11, pp. 88–96.
[6] Shirai, K., Büttner, L., Czarske, J., Obi, S., 2013: “An experimental study on the flow behavior near the read-and-write arm in a hard disk drive model with a shroud opening”, Microsyst. Technol., Vol. 19, pp. 1519-1527.
[7] Ikegawa, M., Mukai, H., Watanabe, M., 2009: “Airflow-simulation by voxel mesh method for complete hard disk drive structure”, IEEE. Trans. Magnet., Vol. 45, pp. 4918-4922.
[8] Dijksman, J.A., Rietz, F., Lörincz, K.A., van Hecke, M., Losert, W., 2012: “Refractive index matched scanning of dense granular materials”, Rev. Sci. Instrum. Vol. 83, 011301.
[9] Westerweel, J., 1997: “Fundamentals of digital particle image velocimetry”, Meas. Sci. Technol., Vol. 8, pp. 1379-1392.